Magnetoresistance oscillation study of the spin counterflow half-quantum vortex in doubly connected mesoscopic superconducting cylinders of Sr_2RuO_4

Xinxin Cai,[1,*] Brian M. Zakrzewski,[1] Yiqun A. Ying,[1] Hae-Young Kee,[2,3] Manfred Sigrist,[4] J. Elliott Ortmann,[5,†] Weifeng Sun,[5,‡] Zhiqiang Mao,[1] and Ying Liu[1,§]

[1]*Department of Physics and Materials Research Institute, Pennsylvania State University, University Park, Pennsylvania 16802, USA*
[2]*Department of Physics, University of Toronto, Toronto, Ontario, Canada M5S 1A7*
[3]*Canadian Institute for Advanced Research, Toronto, Ontario, Canada M5S 1A7*
[4]*Theoretische Physik, ETH Zurich, CH-8093 Zurich, Switzerland*
[5]*Department of Physics, Tulane University, New Orleans, Louisiana 70118, USA*

(Received 9 December 2020; revised 31 December 2021; accepted 26 April 2022; published 21 June 2022)

Vortices in an unconventional superconductor are an important subject for the fundamental study of superconductivity. A spin counterflow half-quantum vortex (HQV) was predicted theoretically for odd-parity, spin-triplet superconductors. Cantilever torque magnetometry measurements revealed previously experimental evidence for HQVs in doubly connected, single-crystal samples of Sr_2RuO_4 with a mesoscopic size. However, important questions on the HQV, such as its stability, have remained largely unexplored. We report in this paper the detection of distinct features in vortex crossing induced magnetoresistance (MR) oscillations in doubly connected, mesoscopic cylinders of single-crystal Sr_2RuO_4, which include a dip and secondary peak in MR, in the presence of a sufficiently large in-plane magnetic field. We argue that these features are due to the formation of spin counterflow HQV in a spin-triplet superconductor, which provides additional evidence for the existence of HQV and insights into the physics of this highly unusual topological object.

DOI: 10.1103/PhysRevB.105.224510

I. INTRODUCTION

The long-range phase coherence of paired electrons in a superconductor gives rise to a superconducting order parameter (OP), which is also the quantum mechanical wave function of these paired electrons. As usual, the gradient of the phase of this wave function is related to the sum of superfluid velocity, v_s, and the vector potential, $\vec{A}$ [1]. The single-valued nature of the wave function requires that the phase winding around a doubly connected superconducting cylinder (obtained by integrating the phase gradient) be $2n\pi$, where n is an integer. Depending on the wall thickness, v_s can be zero or finite in the interior of the cylinder wall, and the flux or fluxoid, the latter of which is the magnetic flux plus a line integral of v_s, will be quantized in units of Φ_0, where $\Phi_0 = h/2e$ is the flux quantum with h the Planck constant and e the elementary charge. Both flux and fluxoid quantizations featuring full-quantum vortex (FQV) fluxoid states were experimentally demonstrated long ago [2–4]).

Half-quantum vortex (HQV) states carrying a magnetic flux of $\Phi_0/2 = h/4e$ are also possible. The concept was proposed originally for spin-triplet superfluid ^{3}He [5,6], for which the OP can be represented by a d-vector. The direction of the d-vector is that against which the Cooper pair spin projection is zero. Its amplitude is the energy gap. It was suggested that the total phase winding, 2π, around a vortex in the condensate can "split" equally between the spin and orbital parts of OP. Since the phase winding in the spin part of the OP does not generate a mass flow, a HQV is obtained. Alternatively, the formation of a HQV can be understood in the so-called "equal-spin pairing" (ESP) state [7] in which the number of spin-up and that of spin-down pairs are the same. When the vorticity is present only in one spin species, which implies the formation of d-vector texture and that of spontaneous spin polarization (SSP), a HQV is found [8].

For a solid-state spin-triplet superconductor, it was proposed that an Abrikosov FQV can split into a pair of HQVs linked by a d-vector soliton [9]. A d-vector texture is created around the soliton with the d-vector reversing its direction going around each end of the soliton, which corresponds to a phase winding of π in the spin part of OP, leading to the formation of a pair of HQVs. The free energy of this topological object was found to depend on the ratio of the ordinary superfluid to spin fluid density, $\frac{\rho_s}{\rho_{sp}}$, where only a large ratio within a narrow range of the temperature below T_c favors the stabilization of the HQV pair [10,11]. In a doubly connected cylinder of a spin-triplet superconductor, a HQV fluxoid state featuring circulating spin and charge currents associated with phase windings in the spin and orbital parts of OP were also predicted [8,10,12]. For a thick-wall cylinder, the Meissner current will flow near the inner surface of the cylinder opposing the circulating current of the HQV to prevent the magnetic field from entering the wall interior. In a thin-wall cylinder,

*Present address: Department of Physics and Astronomy, University of Rochester, Rochester, NY 14627, USA.
†Present address: Department of Physics, University of Texas, Austin, TX 78712, USA.
‡Present address: School of Electrical and Electronic Engineering, Harbin University of Science and Technology, 52 Xue Fu Lu, Nangang, Harbin, 150080 Heilongjiang, China.
§Corresponding author: yxl15@psu.edu

the Meissner current flows in the entire sample, making the HQV a "spin counterflow HQV"—the spin current flows in the direction opposite to Meissner current [13]. Alternatively, a HQV fluxoid state can also form by creating a d-soliton in the cylinder wall and trap $(2m+1)\Phi_0/2$, where m is an integer, in the cylinder [12]. The presence of a d-soliton in the wall leads to a d-vector texture and an SSP, with the latter localized near the soliton (as opposed to the uniform one in the ESP picture) [12].

Cantilever torque magnetometry measurements revealed the formation of the HQV fluxoid state in doubly connected, single-crystal samples of Sr_2RuO_4 with a mesoscopic size [14]. Ramping up the c-axis magnetic field was found to induce a jump in the c-axis magnetization at half-quantum applied flux values, $\Phi = (m + \frac{1}{2})\Phi_0$. The step height was shown to correspond to a FQV based on sample dimensions and the instrumentation calibration. However, in the presence of a sufficiently large in-plane magnetic field (and only in the presence of it), the original jump was seen to be replaced by two half-height jumps near the same applied flux values [14]. However, the same measurements on a control sample of s-wave superconductor, $NbSe_2$, prepared in the same way did not reveal the emergence of two half-height jumps in an in-plane magnetic field [14].

These striking observations were attributed to the formation of a spin counterflow HQV fluxoid state in a spin-triplet superconductor. In this regard, spin-triplet superconductivity in Sr_2RuO_4 was proposed [15,16] soon after its superconductivity was discovered [17], supported by subsequent experiments [13,18–22]. The early Knight shift measurement [23] suggested that the chiral p-wave, E_{2u}, or Γ_5^- state, which features a c-axis oriented d-vector and time-reversal-symmetry breaking (TRSB), is most likely the pairing symmetry realized in Sr_2RuO_4, a conclusion supported further by the early polarized neutron scattering (PNS) measurement [24]. However, new Knight shift measurements on Sr_2RuO_4 [25,26] showed that the constant Knight shift seen in the original measurement [23] was due to the sample being kept in the normal state due to erroneous sample heating. A distinct drop in the Knight shift was found instead as the temperature was lowered [25,26]. A new PNS measurement was also performed, showing now a drop in magnetization that is not as much as that seen in the Knight shift [27]. These new results most likely exclude the Γ_5^- state, but only in the bulk. However, they do not exclude the symmetry-allowed spin-triplet helical states Γ_{1-4}^- [13]. A recent study [28] revealed that the field dependence of the Knight shift down to roughly 0.25 T taken at 25 mK follows closely that of the specific heat, which seems to suggest that the spin susceptibility is dominated by quasiparticles with little contribution from the condensate. This was taken as evidence for even-parity, spin-singlet pairing. However, the condensate should not contribute to the spin susceptibility measured by an in-plane field if Cooper pair spins (in one of the helical spin-triplet states with an in-plane d-vector) are locked to the c axis due to spin-orbital coupling, a possibility not yet considered [28].

The symmetry of the OP can be probed independently by Josephson effect based experiments, the phase-sensitive measurement proposed originally by Geshkenbein, Larkin, and Barone (GLB) [29]. This experiment relies on using a hybrid superconducting quantum interference device (SQUID) consisting of two oppositely faced Josephson junctions between a spin-singlet s- and spin-triplet p-wave superconductor to detect the change in the phase of OP after a 180-degree rotation. The Josephson couplings of the two junctions will be of opposite signs because of the phase change of π after 180-degree rotation. Using the $Au_{0.5}In_{0.5}$-Sr_2RuO_4 GLB SQUID, the phase-sensitive experiment [30] showed a minimum at zero total applied magnetic flux ($\Phi = 0$) in the $I_c(\Phi)$ oscillations when the temperature approaches the T_c of the SQUID. In a control sample with the two Josephson junctions in the SQUID prepared on the same surface, a maximum in $I_c(\Phi)$ was found at $\Phi = 0$. These observations are consistent only with an odd-parity, spin-triplet pairing symmetry. Various questions on the original phase-sensitive experiment have been addressed since then [13].

Therefore, despite the current controversy on the pairing symmetry in Sr_2RuO_4, the original interpretation of the observed HQV fluxoid state in a spin-triplet picture did not seem to be invalidated. Further experimental work seeking additional evidence for HQV in mesoscopic Sr_2RuO_4 will help settle not only the existence of spin counterflow HQV but also the spin-triple pairing symmetry. Moreover, important questions related to HQV itself remain to be addressed. For example, opposite to the original theoretical prediction [10], the mesoscopic sample size alone was shown in the magnetometry experiment to be insufficient to stabilize the HQV. The stability of HQV is ensured by the additional free energy lowering through the coupling between the in-plane field and the SSP, which lowers the free energy of the HQV by $\Delta F = -\mu_x|\mu_0 H_{||ab}|$, where μ_x is the in-plane spontaneous magnetization and μ_0 is vacuum permeability.

Magnetoresistance (MR) oscillation measurements on a multiply connected, perforated thin film of Sr_2RuO_4 were proposed as an alternative method for the detection of spin counterflow HQV [31]. Early MR measurements on Sr_2RuO_4 cylinders of a mesoscopic size in the absence of an in-plane field yielded no clear evidence for the HQV fluxoid state [32]. Here we show that MR measurements on mesoscopic Sr_2RuO_4 with an in-plane field did yield evidence for the HQV fluxoid state and, therefore, spin-triplet pairing in this material.

II. EXPERIMENTAL METHODS

High-quality single crystals of Sr_2RuO_4 were grown by the floating-zone method. Thin crystals of Sr_2RuO_4 were obtained by mechanical exfoliation as reported previously [32]. The typical lateral dimension of our thin crystals, one of which is shown in Fig. 1(a), is 10–50 μm with a thickness 300–800 nm. Electrical contacts to a thin crystal placed on a Si/SiO_2 substrate were patterned by photolithography. Electron beam evaporation was used to deposit 10 nm thick Ti followed by 200 nm thick Au after a brief ion milling of the crystal surface. Ti/Au contacts were evaporated from an angle (about 45° to the normal of the substrate) to ensure continuous coating of the metals on the side surfaces of the crystal. A 200 nm thick SiO_2 was deposited on the top of crystal plate as a protective layer before a doubly connected cylinder with

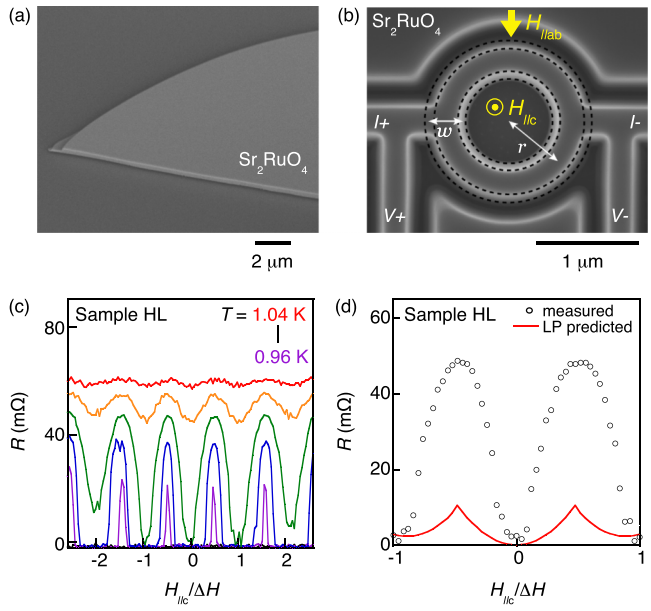

FIG. 1. Sample preparation and MR oscillations. (a) A scanning electron microscope (SEM) image of a thin single crystal of Sr_2RuO_4 obtained by mechanical exfoliation. (b) SEM image of a FIB-cut doubly connected cylinder of Sr_2RuO_4 with four measurement leads. Directions of c-axis and in-plane magnetic fields, $H_{||c}$ and $H_{||ab}$, respectively, are indicated. (c) Sample resistance, R, vs $H_{||c}$, the MR at $T = 0.96$, 0.98, 1.00, 1.02, and 1.04 K for sample HL at $H_{||ab} = 0$. Here $R = [V(I = I_m) - V(I = 0)]/I_m$, $I_m = 10\ \mu$A, and $\Delta H_{||c} = 15.4$ Oe. (d) MR oscillations measured at $T = 1$ K (open circles) and those calculated from the Little-Parks (LP) effect (solid lines) using the sample dimensions and the slope of $R(T)$ measured at $I_m = 10\ \mu$A.

four electrical leads was cut by a focused ion beam (FIB) enabled by 30 keV Ga ions with a beam current of 50 pA. A typical sample is shown in Fig. 1(b). The cylinder axis is along the c axis of Sr_2RuO_4.

In the original magnetometry experiment, the doubly connected samples of Sr_2RuO_4 featured a large and uneven wall thickness with only the central hole cut by FIB [14], probably due to concerns on potentially destroying superconductivity by the high-energy FIB. For samples used in the present work, both the inner and outer edges of the cylinder were cut by FIB to form the cylinder that is appropriate for the electrical transport measurements. The use of the 200 nm thick protective layer of SiO_2 was important for preventing conducting material cut off from the crystal from being redeposited directly on the top of the cylinder that may affect our transport measurements, minimizing also the damage of the cylinder from the (nonmagnetic) Ga implantation.

Previous transmission electron microscope (TEM) studies of FIB-cut Sr_2RuO_4 cylinders [32] revealed that the cylinder wall features a gradually decreasing hole diameter from top to bottom, which is expected because the upper part of the crystal was exposed to the FIB longer than the lower part. The inner and the outer walls of the cylinder were found in addition to feature a FIB-damaged surface layer of about 10 nm thickness, which is most likely to be non-superconducting given the sensitivity of superconductivity in Sr_2RuO_4 to disorder. The damaged surface layers were not removed in the current experiment by low-energy Ar ion milling as was done in the preparation of Josephson junctions. The presence of this non-superconducting layer is unlikely to introduce any complications. The dimensions of the cylindrical samples listed in Table I, obtained from scanning electron microscope (SEM) images, are given with two 10 nm surface layers taken out.

Our samples were measured in a dilution refrigerator with a base temperature of 20 mK. Four-point resistance, obtained via a standard dc technique using a measurement current of I_m, was calculated by $R = [V(I = I_m) - V(I_m = 0)]/I_m$. The current was supplied by a Keithley 220. The voltage across the sample was measured using a Keithley 2182. The voltage offset at $I_m = 0$, which may come from sources such as contacts between two different materials, Au/Ti and Sr_2RuO_4, as well as background signals in the measurement circuitry, is subtracted to obtain the true response of the sample to the measurement current flowing through the sample in the specified direction.

An in-plane magnetic field, $H_{||ab}$, was applied by a superconducting solenoid magnet. A c-axis magnetic field, $H_{||c}$, was applied using a pair of homemade superconducting Helmholtz coils installed inside the large superconducting solenoid. The current in the Helmholtz coil was provided by a Keithely 2400 SourceMeter, generating a magnetic field about 30.8 Oe per 0.1 A of magnet current. The sample planes were aligned manually with respect to the magnetic field directions as precisely as possible. A typical misalignment of 1–2 degrees, possibly larger in rare cases, is expected.

The applied magnetic flux enclosed in the cylinder, denoted by Φ, is calculated from the c-axis magnetic field, $H_{||c}$, and sample dimensions. The period in $H_{||c}$ for the primary MR oscillations of the period of Φ_0 is calculated using the relation

TABLE I. Summary of sample parameters. Sample sizes including midpoint radius r, wall thicknesses of the cylinder at the top (w_1) and the bottom (w_2), and the cylinder height h were estimated from SEM images. Other parameters including the zero-resistance and onset transition temperature, $T_{c,R=0}$ and $T_{c,\text{onset}}$, and values of the critical current density at a fixed temperature, J_c, were obtained from electrical transport measurements.

Sample	r_m (nm)	w (nm)		h (nm)	T_c (K)		J_c (10^3 A/cm^2)
		Top	Bottom		$R = 0$	Onset	
HL	601	191	334	780	0.99	$\geqslant 1.63$	8.6 at $T = 0.5$ K
BL	468 (full: 534)	133 (full: 268)	283 (full: 414)	644	1.18	$\geqslant 1.4$	24 at $T = 0.3$ K
E	565	190	298	482	0.71	$\geqslant 1.35$	92 at $T = 0.3$ K
B	597	183	322	540	1.04	2.1	75 at $T = 0.55$ K

$\Delta H_{||c} = \Phi_0/\{\pi r^2[1 + (\frac{w}{2r})^2]\}$, where r is the midpoint radius. A correction term of order $(\frac{w}{2r})^2$ will also be included using an average wall thickness w [33]. Experimentally, $\Delta H_{||c}$ was determined from the average of peak-to-peak and valley-to-valley values of the first period at the highest temperature for which MR oscillation data is available for the sample because MR oscillations under these conditions were most smooth.

For mesoscopic samples of Sr_2RuO_4, the onset T_c can sometimes be higher than the bulk. The enhanced T_c could be related to the presence of Ru inclusions, uniaxial strains, and/or dislocations [34], or, as to be discussed below, the multiple branching in the sample. No Ru inclusions were seen in our samples in optical or SEM imaging. The absence of Ru inclusions is consistent with the fact that thin crystals of Sr_2RuO_4 can be obtained by mechanical exfoliation only in crystals with a stoichiometry that is either optimal or slightly Ru deficient. Ru-rich crystals of Sr_2RuO_4 cannot be cleaved.

III. RESULTS

A. Vortex crossing induced MR oscillations

We measured sample resistance R as a function of $H_{||c}$ in zero $H_{||ab}$ and obtained pronounced MR oscillations, shown in Fig. 1(c). The period of the MR oscillations, $\Delta H_{||c}$, is in good agreement with that estimated from Φ_0 using sample dimensions listed in Table I. It is known that the amplitude of LP MR oscillations is $\Delta R(T) = \Delta T_c(dR/dT)$, where dR/dT is the slope of the R vs T curve in the transition region and ΔT_c is readily found in the literature [32,33]. However, as shown in Fig. 1(d), the amplitude of the MR oscillations of our sample is much larger than that expected from the LP effect [4,33]. The MR oscillations were also found to persist down to very low temperatures, as seen previously [32]. These features suggest that MR oscillations seen here are due to vortex crossing rather than the LP effect, as seen previously [32]. Vortex crossing induced MR oscillations were studied extensively in doubly connected samples of type II s-wave superconductors [35–37].

Abrikosov FQV or HQV should be allowed in a cylinder wall thicker than twice the zero-temperature superconducting coherence length, $2\xi_{ab}(0) \approx 132$ nm, when $H_{||c}$ is larger than the lower critical field. Driven by the total current, the sum of circulating and measurement currents, $I_s + I_m$, an Abrikosov FQV or HQV will cross the sample, overcoming a free-energy barrier. Such crossing leads to a phase slip of π for HQV or 2π for FQV, which in turn leads to a finite voltage V in the direction perpendicular to the direction of vortex crossing. According to the Josephson relation, V is proportional to the rate of vortex crossing that depends on I_m nonlinearly [1]. The sample resistance R is given by V/I_m for a specified I_m. Because the free-energy barrier for vortex crossing is a periodic function of applied magnetic flux Φ, R varies periodically with Φ as well, resulting in MR oscillations.

Vakaryuk and Vinokur [31] calculated vortex-crossing induced MR oscillations for a multiply connected film of Sr_2RuO_4 treated as an array of heavily damped Josephson junctions in the Ambegaokar and Halperin (AH) model [38]. The MR is then given by

$$R/R_N = I_0^{-2}(\Delta E/2k_BT), \quad (1)$$

where R_N is the normal-state resistance, ΔE the free-energy barrier, and $I_0(x)$ is a zero-order modified Bessel function of the first kind [31].

The fluxoid state of a doubly connected spin-triplet cylinder is denoted by (n_s, n_{sp}), where n_s and n_{sp} are the phase winding numbers for the orbital and spin parts of OP, respectively. n_s and n_{sp} can be a whole or half integer, but their sum must be an integer to ensure that the total phase winding is multiple of 2π. Vortex crossing leads to a fluxoid state transition from the initial state of (n_s, n_{sp}) to (n_s', n_{sp}') after the FQV or HQV that enters the cylinder wall exits it, turning into magnetic flux enclosed in the cylinder. More precisely, the fluxoid state transition occurs when the Abrikosov HQV or FQV reaches roughly the midpoint in the cylinder wall. After the enclosed magnetic flux forms a FQV or HQV in the cylinder wall on the other side and exits it, the fluxoid state returns to (n_s, n_{sp}).

B. Free-energy barrier for vortex crossings

The free-energy barrier for vortex crossing through a doubly connected cylinder of a spin-triplet superconductor is yet to be calculated. However, essential features of this barrier may be inferred from the analysis of the corresponding problem in a conventional s-wave superconductor performed in the London limit [39]. As shown in the Supplemental Material (SM) [40], this free-energy barrier as a function of the vortex position in the cylinder wall, x, for fixed values of Φ and I_m consists of three segments: Segment 1 is the free energy for the FQV or HQV in the cylinder wall on the "entry" side. Its maximal value will be denoted as ΔE_{in}. Segment 2 is the change in the free energy associated with the fluxoid state transition from (n_s, n_{sp}) before to (n_s', n_{sp}') after the FQV or HQV enters the interior of the cylinder, and $\Delta E_{fl} = F(n_s', n_{sp}') - F(n_s, n_{sp})$. Segment 3 is the free energy of the vortex in the cylinder wall on the opposite side, with ΔE_{out} the maximal free energy relative to that of (n_s', n_{sp}'). The system returns to (n_s, n_{sp}) at the end.

The free-energy barrier will be tilted by I_m because of the work done by the Lorentz force. Assuming that I_m is distributed symmetrically between two sides of the cylinder wall, ΔE_{in} will be the maximal value of the position-dependent free-energy barrier in the limit of large I_m (see SM [40]), which suggests that ΔE_{in} would dominate the vortex crossing rate. As Φ varies, so does ΔE_{in}, leading to MR oscillations. Time-dependent Ginzburg-Landau analysis of the vortex crossing in an s-wave superconductor yielded a similar result [36]. Interestingly, the Φ dependence of ΔE_{in} follows that of ΔE_{fl}, which is reasonable—in the thin-wall limit in which the vortex formation in the cylinder wall is not allowed, the free-energy barrier will be determined solely by ΔE_{fl}. The MR can be calculated using Eq. (1) where ΔE_{fl} will be the free-energy barrier. The dependence of ΔE_{fl} on Φ will then be "mapped" into the MR oscillations in the limit of large I_m. Importantly, different from both ΔE_{in} and ΔE_{out}, the Φ dependence of ΔE_{fl} is known for a spin-triplet superconducting cylinder [10]. Taking advantage of this result, we will use features seen in MR oscillations to infer the Φ dependence of ΔE_{fl}, which will reveal the signature for HQV.

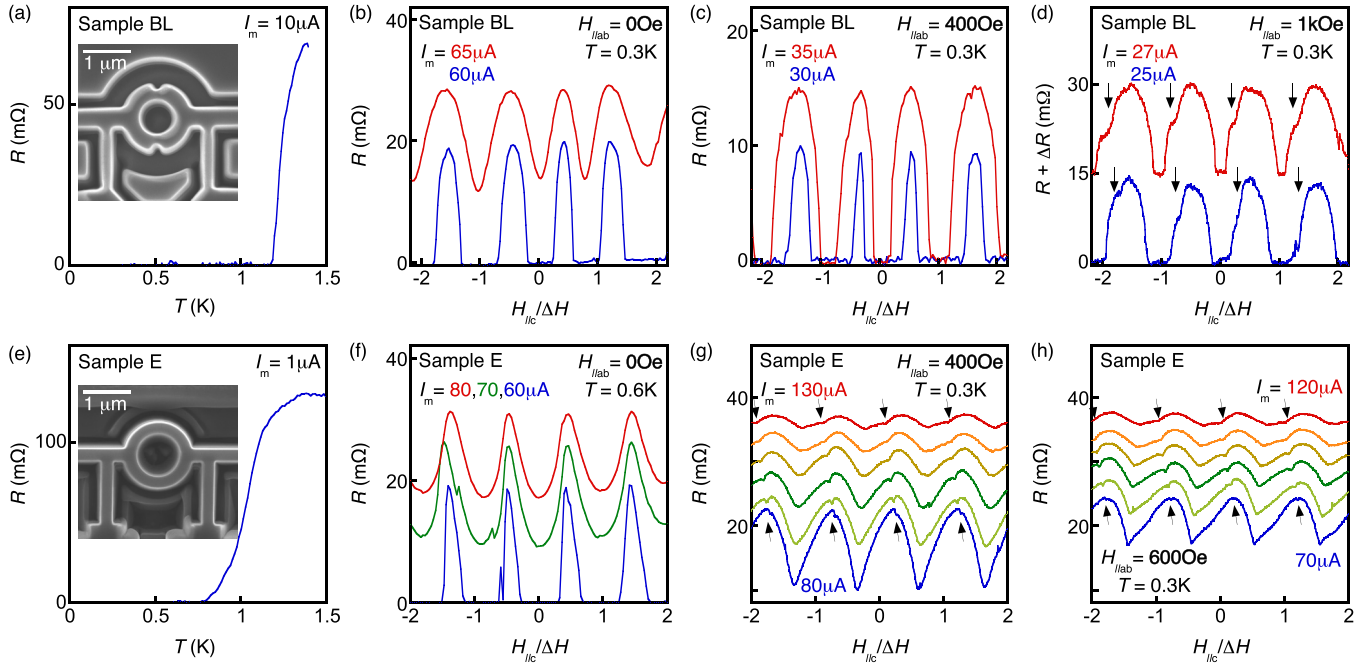

FIG. 2. Dip feature in MR oscillations. (a) Sample resistance, R, vs temperature, T, for sample BL, measured at $I_m = 10\ \mu$A and zero field. Inset: SEM image of the sample featuring two constraints. (b)–(d) R vs $H_{||c}$ measured at fixed in-plane magnetic fields, $H_{||ab} = 0$ (b), 400 (c), and 1000 Oe (d) with values of I_m indicated. The top curve in (d) is shifted vertically by 15 mΩ for clarity. $\Delta H_{||c} = 19.7$ Oe for sample BL. (e) R vs T of sample E at zero magnetic field measured at $I_m = 1\ \mu$A. Inset: SEM image of the sample. (f)–(h) R vs $H_{||c}$ obtained at fixed in-plane fields of $H_{||ab} = 0$ (f), 400 (g), and 600 Oe (h) with values of I_m indicated in (f). For (g) and (h), the values of I_m are, from top to bottom, 130, 120, 110, 100, 90, and 80 μA in (g) and 120, 110, 100, 90, 80, 70 μA in (h). $\Delta H_{||c} = 18.8$ Oe for sample E. Except for (d), no shift was made in all other plots. The dip features are indicated by arrows.

C. In-plane magnetic field induced dip feature

The free energy of the HQV fluxoid state in a doubly connected cylinder depends on the wall thickness. It was shown that for a cylinder featuring constrictions, sections of the wall thinner than rest of it, the free-energy barrier for vortex crossing is determined by the smallest wall thickness [14]. The use of such a sample could help minimize sample damage from high-energy FIB. We prepared a cylinder, sample BL, featuring two constrictions [inset of Fig. 2(a)]. R vs $H_{||c}$ data at fixed in-plane fields obtained using different I_m revealed pronounced MR oscillations with a period of Φ_0 [Figs. 2(b)–2(d)]. A small but clear dip feature is seen in MR oscillations at $H_{||ab} = 1000$ Oe [indicated by the arrows in Fig. 2(d)], which is not seen at $H_{||ab} = 0$ [Fig. 2(b)] or 400 Oe [Fig. 2(c)].

Another sample, sample E, which possesses a uniform wall thickness comparable with that of the constrictions in sample BL, was prepared and found to show robust superconductivity with a somewhat lower T_c than sample BL [Fig. 2(e)]. At $H_{||ab} = 0$, only smooth MR oscillations with a period of Φ_0 were observed [Fig. 2(f)]. While minimal values of MR at $H_{||ab} = 0$ appear to locate near $\Phi = m\Phi_0$, where m is an integer [Fig. 2(g)], as expected, for $H_{||ab} = 400$ and 600 Oe, MR minima were seen to be moving away from $\Phi = m\Phi_0$, which could be due to a misalignment of $H_{||ab}$ even though an intrinsic physical origin cannot be excluded. Most importantly, at $H_{||ab} = 400$ and 600 Oe, a dip is again seen clearly, as indicated by arrows in Figs. 2(g) and 2(h).

Systematic behavior of the dip, in particular, the effect of I_m on it, was observed. First, at a fixed I_m, the dip is seen to locate on the same side of the MR peak independent of the sign of $H_{||c}$. When the direction of I_m is reversed, the dip switches from one side of the main MR peak to the other [Figs. 3(b) and 3(c)]. Second, the position at which the dip was found, referred to as $\Phi = \Phi_m$, which is very close to the center of the main MR peak at small values of I_m, moves away from the center as I_m was increased [Fig. 3(c)]. Finally, the amplitude of MR oscillations was found to depend not only on the magnitude but the direction of I_m as well [Fig. 3(c)]. All this suggests that I_m plays a crucial role in determining the rate of vortex crossing, as to be discussed below.

D. Signature for the HQV fluxoid state

We argue below that the dip feature seen in Fig. 2 is due to HQV crossings overcoming a free-energy barrier which is a periodic function of $\Phi = \pi r^2 H_{||c}$. Consider now the free energy of the fluxoid state of a doubly connected cylinder of a spin-triplet superconductor featuring a layered structure and $w \ll r, \lambda_{ab}$, where λ_{ab} is the in-plane penetration depth (for a field applied along the c axis). The kinetic-energy (or phase-gradient) part of the free energy per cylinder length with I_m set to zero is [10]

$$F(n_s, n_{sp}) = \left(\frac{\Phi_0^2}{8\pi^2 r^2}\right)\beta\left[\frac{1}{1+\beta}\left(n_s - \frac{\Phi}{\Phi_0}\right)^2 + \frac{\rho_{sp}}{\rho_s} n_{sp}^2\right], \tag{2}$$

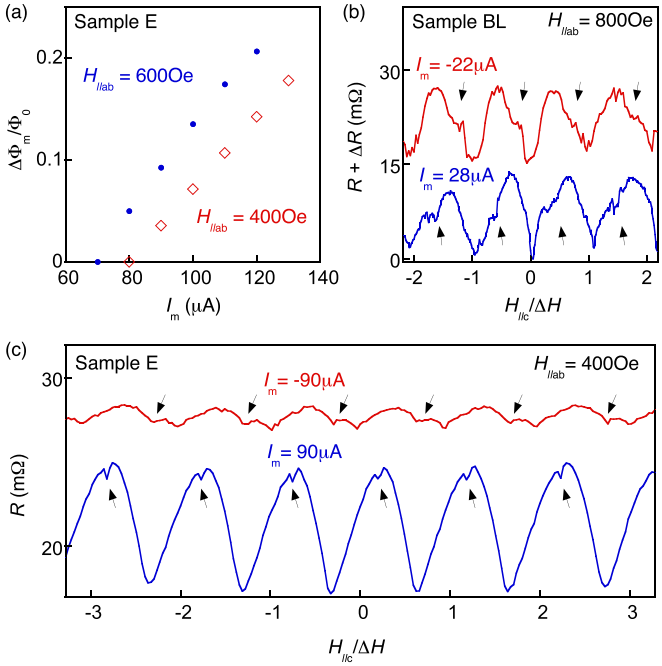

FIG. 3. Effect of I_m on the dip. (a) Position of the dip ($\Phi = \Phi_m$) vs I_m for sample E obtained at $H_{||ab} = 400$ and 600 Oe. The shift is measured from the maximum of the MR peak. (b), (c) R vs $H_{||c}$ obtained at a fixed $H_{||ab}$ and I_m as indicated for samples BL and E. The top curve in (b) is shifted vertically by 15 mΩ for clarity. Reserving the direction of I_m leads to a shift of the dip in the MR oscillations from one side of the main MR peak to another (indicated by the arrows) as well as a significant change in the amplitude of MR oscillations for sample E.

where ρ_s and ρ_{sp} are the superfluid and spin fluid densities, respectively, and $\beta = rw/(2\lambda_{ab}^2)$. It is seen from Eq. (2) that the free-energy difference between a HQV (n_s = half integer) and FQV (n_s = integer) fluxoid state depends on the relative values of ρ_{sp}/ρ_s and $(1+\beta)^{-1}$, which depend on material- and/or sample-specific properties as well as the temperature. As noted above, a thin cylinder wall with a small w will help lower the free energy of the HQV fluxoid state. The free-energy formula shown in Eq. (12) of Ref. [10] has an additional $(\Phi/\Phi_0)^2$ term, which will not make any difference in $\Delta E_{\rm in}$, ΔE_{fl}, or $\Delta E_{\rm out}$ at a fixed Φ as only changes in the free energy between two different fluxoid states are relevant here.

We now plot the circulating supercurrent I_s in the fluxoid ground state as a function of applied Φ for three combinations of ρ_{sp}/ρ_s and $(1+\beta)^{-1}$ [Figs. 4(a)–4(c), upper panels]. It is seen that I_s reverses sign below and above $\Phi = (m+\frac{1}{2})\Phi_0$ as phase winding numbers are changed [Figs. 4(a) and 4(b), upper panels], resulting in the system entering/exiting the HQV fluxoid state [Fig. 4(c), upper panel]. The c-axis magnetization will change its sign accordingly, which enabled the detection of HQV fluxoid states in the original magnetometry experiment [14]. For Fig. 4(a), $(\rho_{sp}/\rho_s)/(1+\beta)^{-1} = 3.08$, the FQV fluxoid state is energetically favored over the HQV one at all values of Φ. In Fig. 4(b), $(\rho_{sp}/\rho_s)/(1+\beta)^{-1} = 1.8$, the free energy of the HQV fluxoid state is seen to be lowered in comparison with that shown in Fig. 4(a). The free energy of the HQV fluxoid state is lowered further if we set $(\rho_{sp}/\rho_s)/(1+\beta)^{-1} = 0.52$.

Note that $H_{||ab}$, whose effect was not considered in Eq. (2), will help push down the free energy of the HQV fluxoid states because of the coupling between the SSP accompanying the HQV fluxoid state and $H_{||ab}$ [8,41]. Indeed, the same amount of lowering of the free energy seen in Fig. 4(c) can be achieved alternatively by applying an in-plane field with the same values of ρ_{sp}/ρ_s and $(1+\beta)^{-1}$ used in Fig. 4(b). As a result, a sufficiently large $H_{||ab}$ can make the free energy of the HQV fluxoid state lower than that of FQV near $\Phi = (m+\frac{1}{2})\Phi_0$ as long as the value of $(\rho_{sp}/\rho_s)/(1+\beta)^{-1}$ is reasonably large, making either the HQV or the FQV fluxoid state the ground state as Φ is varied [Fig. 4(c)].

Crossing of a HQV or FQV causes a transition from the ground to the first-excited fluxoid state, as indicated in Figs. 4(a)–4(c). Here blue arrows mark transitions in which a FQV crosses and n_s changes by 1, and red arrows mark those with n_s changing by 1/2 induced by the crossing of a HQV. Note that transitions from the first-excited back to the ground fluxoid state are not shown in Figs. 4(a)–4(c) to avoid overly busy figures. In Figs. 4(d)–4(f) (upper panels), values of the excitation energy from the ground to the first-excited fluxoid state, ΔE_{fl}, are plotted against Φ. While the free energy of the fluxoid state itself is a quadratic function of Φ, the excitation energy is a linear function of Φ. Values of MR, shown in Figs. 4(d)–4(f) (lower panels), were calculated using Eq. (1) for which $\Delta E = \Delta E_{fl}(\Phi)$. The presence of I_m tilts the free-energy barrier as a function of the vortex position, making ΔE_{fl} dominate MR oscillations.

Features in the free-energy barrier lead to corresponding features in MR oscillations. In Fig. 4(d), the vortex crossing induced MR oscillations are conventional (lower panel). In Fig. 4(e) (upper panel), the free-energy barrier for vortex crossing as a function of Φ has a kink at the point where the free-energy parabola of the FQV and that of the HQV fluxoid states coincide as shown in Fig. 4(b) (lower panel), which results in a kink in MR oscillation as well [Fig. 4(e), lower panel]. However, this subtle change of slope in MR is unlikely to be observed experimentally. Finally, when the free energy of HQV fluxoid states is substantially lowered by either a large value of $(\rho_{sp}/\rho_s)/(1+\beta)^{-1}$ or a sufficiently large $H_{||ab}$ as shown in Fig. 4(c), HQV fluxoid states near $\Phi = (m+1/2)\Phi_0$ become the ground states. A peak was found in ΔE_{fl}, leading to a dip in MR [Fig. 4(f)], as seen experimentally (Fig. 2).

The results shown in Fig. 3 can also be accounted for if the formation of the HQV fluxoid state is due to that of a d-soliton in the cylinder wall accompanied by the trapping of half-quantum flux in its interior [12]. In this picture, the SSP is formed locally near the soliton rather than uniformly in the entire sample predicted for the ESP-based model [31]. A d-vector texture is expected in both models. A Ginzburg-Landau theory formulated for the d-soliton HQV includes only the radial component of SSP, s_r, by choosing a specific gauge. Importantly, the HQV fluxoid state can be stabilized by $H_{||ab}$ even if the d-vector is not along the c axis away from the soliton [12]. The presence of an s_r leads to a shift in the free-energy parabolas for the HQV fluxoid state [12]. The parabolas now reach the minimum at $\Phi = (m+\frac{1}{2})\Phi_0 + \Phi_m$,

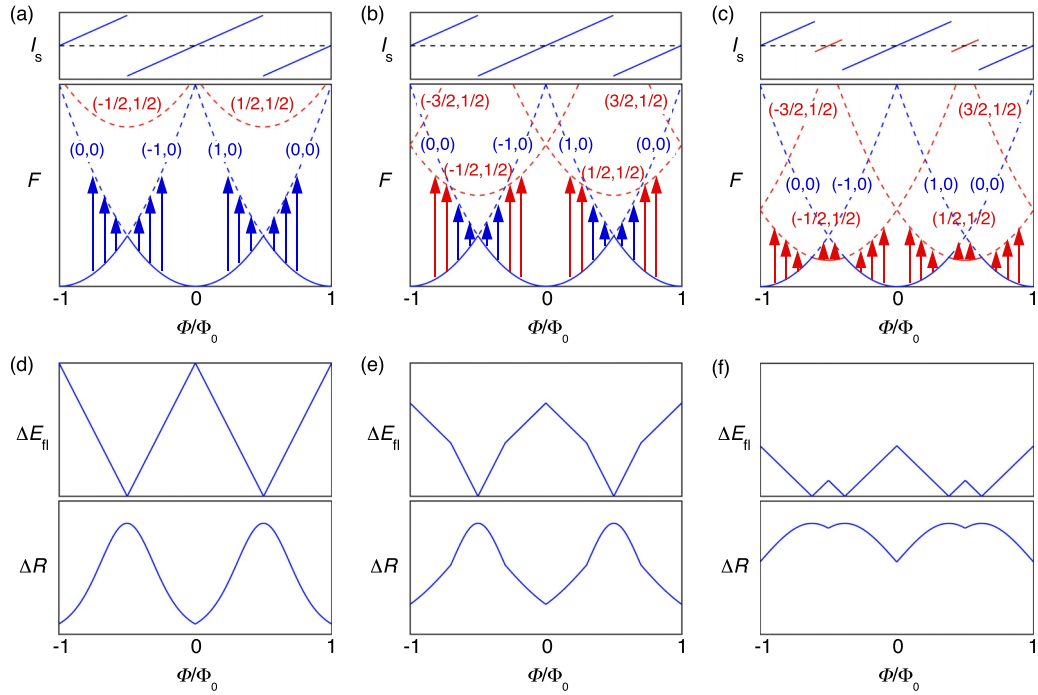

FIG. 4. Fluxoid-state free energy and MR oscillations. (a)–(c) Circulating supercurrent I_s (upper panels) and the kinetic-energy part of the free energy F (lower panels) of a doubly connected cylinder of a spin-triplet superconductor in a fluxoid state (n_s, n_{sp}) as a function of Φ calculated using Eq. (2). The dashed line in the upper panels indicates the zero value of I_s. Three different combinations of ρ_{sp}/ρ_s and $(1+\beta)^{-1}$ values were used to calculate the free energy (see main text). When the free-energy parabolas for the HQV fluxoid state are lowered sufficiently by geometrical constraints and/or the application of $H_{||ab}$, the HQV fluxoid state become the "ground" state near $\Phi = \pm\Phi_0/2$ (red solid lines). A transition from the "ground" to "first excited" fluxoid state at a fixed Φ is seen, as indicated by arrows (blue for FQV and red for HQV). The transition is accompanied by the entry of a FQV or HQV into the interior of the cylinder. Returning from the "first excited" to the "ground" fluxoid state corresponds to the exit of a FQV or HQV on the other side of the cylinder (no arrows are shown). (d)–(f) Upper panels: Values of the "excitation energy" between the "ground" and the "first excited" fluxoid state, $\Delta E_{fl}(\Phi)$, computed from the free-energy differences shown in (a)–(c) (lower panels). Lower panels: The expected MR oscillations, $\Delta R(\Phi)$, calculated using Eq. (1) with $\Delta E = \Delta E_{fl}$. In (f), HQV crossings are seen to lead to a dip in main peaks of MR oscillations.

with the magnitude of Φ_m proportional to the square root of the strength of the spin-orbit coupling and s_r. This shift will in turn lead to a shift in the dip away from $\Phi = (m + \frac{1}{2})\Phi_0$. As shown in Figs. 2(g) and 2(h), the dip in the MR oscillations at a fixed I_m in sample E is seen to locate on the same side of the MR peak, independent of the sign of $H_{||c}$, consistent with the d-soliton picture: Since Φ_m is independent of Φ, the resulting shift in the dip feature at a fixed I_m should also be independent of the sign of Φ. Given that the spin-orbital coupling is unlikely to be affected by I_m, the switching of the dip position from one side of the main MR peak to the other when the direction of I_m was reversed, a trend seen in both samples BL and E [Fig. 3(b)], providing additional support to our argument that the shift of the dip as I_m is varied is due to I_m affecting s_r.

The position of the dip is seen to shift away from the maximal values of main MR peak at $\Phi = (m + \frac{1}{2})\Phi_0$ as I_m is increased [Fig. 3(a)]. This shift in the dip position is consistent with the d-soliton picture as well. Assuming that I_m is distributed asymmetrically between two sides as well as along the axis of the cylinder, the z axis, the resulting circulating current, $I_{m,cir}$, will feature a magnitude depending on z. In addition, in the London limit, the supercurrents flowing through a superconductor tend to concentrate near the sample surface. Because of the uneven thickness of the cylinder wall (thinner on the top and thicker at the bottom; see SM [40]), $I_{m,cir}$ will not flow through the cylinder uniformly, leading to a magnetic field that features a radial component according to the Biot-Savart law. Indeed, for an infinitely long, uniform solenoid, the magnetic field will be along the axis of the cylinder with zero radial component. For an infinitely thin loop, on the other hand, the current-generated magnetic field will feature a large radial component. If $I_{m,cir}$ is concentrated at the bottom surface of the cylinder, it will generate a radial component of the magnetic field in the rest of the sample. As a result, when I_m reverses its direction, the direction of the radial component of the field will be reversed as well, which may also reverse s_r; when I_m is increased in magnitude, s_r will increase accordingly. Taking into account of all this, the dip position seen in Fig. 3(a) appears to be consistent with the d-soliton picture featuring an s_r tuned by I_m.

E. Secondary peaks in MR oscillations

The dip feature in MR oscillations that is linked to the HQV fluxoid state is seen so far to be most prominent in a sample showing the largest J_c. Sample B, another cylinder whose parameters are shown in Table I, was found to also feature a large J_c. Different from other samples, however, this sample possesses an enhanced value of onset T_c.

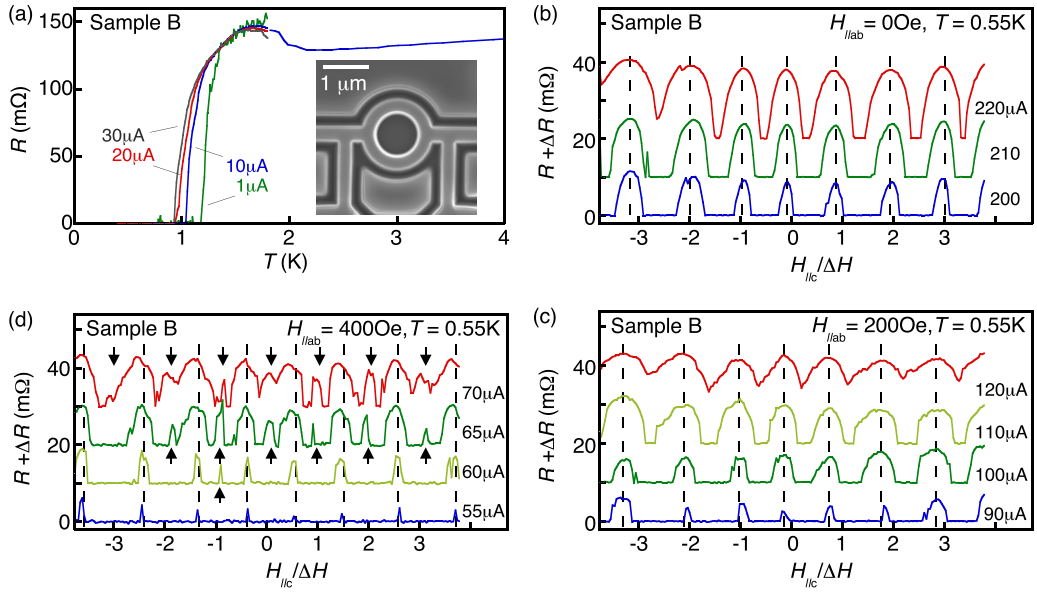

FIG. 5. Secondary peaks in MR oscillations at integer applied flux quanta. (a) Sample resistance (R) vs temperature (T) for sample B, measured in zero magnetic field and at various I_m values as indicated. Inset: SEM image of the sample. R vs $H_{||c}$ curves obtained at a fixed in-plane field of $H_{||ab} = 0$ (b), 200 (c), and 400 Oe (d) are shown with values of I_m indicated. $\Delta H = 16.3$ Oe (corresponding to Φ_0). Except the lowest curves, all others in (b)–(d) are shifted vertically by 10 Ω for clarity. The MR oscillations with a period of Φ_0 are indicated by dashed lines. The secondary peaks in MR oscillations found near integer applied flux quanta at $H_{||ab} = 400$ Oe are indicated by arrows in (d).

As shown in Fig. 5(a), curves of R vs T obtained from this sample in zero magnetic field at various I_m values feature an anomalous resistance peak. The existence of such a resistance anomaly was seen previously in mesoscopic samples of conventional s-wave superconductors that feature an enhanced local T_c near voltage leads [42,43]. As the temperature is lowered, the initial rise in the sample resistance signals the largest local T_c and superconducting energy gap. Given that no Ru inclusions that are known to feature an enhanced local T_c up to 3 K [44] were seen in our samples as discussed above, the enhancement in the local T_c in sample B must be due to a combination of the branching and the existence of dislocations that were found previously to lead to T_c enhancement [34]. Because of the enhanced gap value, even though only locally, the overall free-energy barrier for the vortex crossing should be larger than other samples. Nevertheless, prominent MR oscillations with a period of Φ_0 were observed in this sample at $H_{||ab} = 0$ and 200 Oe. However, no dip feature was found. At $H_{||ab} = 400$ Oe, again no dips were seen. However, secondary MR peaks between two adjacent main MR peaks were found around integer applied flux quanta, $\Phi = (m + \frac{1}{2})\Phi_0$ [Fig. 5(d)]. The period for the MR oscillations is seen to change from $\Phi_0 = h/2e$ to $\frac{1}{2}\Phi_0 = h/4e$.

We argue below that secondary peaks in MR oscillations are expected near $\Phi = m\Phi_0$ if transitions from the FQV ground to HQV first-excited fluxoid state and the trapping of the latter are allowed [Fig. 6(a)], which requires that free-energy parabolas for HQV fluxoid states be lowered sufficiently because either $(\rho_{sp}/\rho_s)/(1+\beta)^{-1}$ or $H_{||ab}$ is sufficiently large, or both. In addition, transitions from the ground to the first-excited fluxoid state near $\Phi = (m + \frac{1}{2})\Phi_0$ will also be possible. As shown above, for transitions corresponding to an increase or a drop in n_s by 1/2 or 1, a HQV or FQV will enter or exit the cylinder. The follow-up transitions from the trapped first-excited to second-excited fluxoid state will result in a main MR peak near $\Phi = (m + \frac{1}{2})\Phi_0$ or a secondary one near $\Phi = m\Phi_0$ in MR oscillations, overcoming their respective free-energy barriers. Importantly, as seen in Fig. 6(b), the free-energy barrier for fluxoid state transitions near $\Phi = (m + \frac{1}{2})\Phi_0$ features no peak as seen in Fig. 4(f)

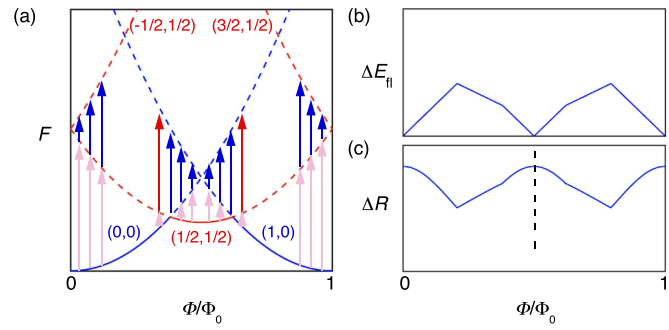

FIG. 6. Fluxoid-state trapping and consequence in MR oscillations. (a) Free-energy parabolas for fluxoid states of (n_s, n_{sp}) in a large in-plane field as shown in Fig. 4(c) with the trapping of a HQV/FQV fluxoid state also considered. A HQV "first excited" fluxoid state near $\Phi = m\Phi_0$ and a FQV one near $\Phi = (m + \frac{1}{2})\Phi_0$ resulting from a FQV or HQV crossing may be trapped, with the transition indicated by the light red or blue arrows. Follow-up transitions from the "first excited" to "second excited" fluxoid state are indicated by red/blue arrows that are again accompanied by a FQV/HQV crossing. (b) Upper panel: The "excitation energy" as function of Φ for fluxoid state transitions shown in (a), taking into account the trapping of fluxoid state. Lower panel: Expected MR oscillations. Phase slip rate from the crossing of HQV and that from the FQV are not distinguished. MR was calculated using Eq. (1).

(upper panel), which will lead to no dip features in the main MR peaks [Fig. 6(b)], as seen experimentally.

A small and/or asymmetrically distributed I_m will help make $\Delta E_{\rm in}$ not the maximum of the position-dependent free-energy barrier (see SM [40]) and trapping a fluxoid state relatively easy, especially when $\Delta E_{\rm out}$ is comparable to or larger than $\Delta E_{\rm in}$. For a doubly connected cylinder of a conventional, layered s-wave superconductor, both $\Delta E_{\rm in}$ and $\Delta E_{\rm out}$ at $I_m = 0$ depend on λ_{ab}^2 ($\sim\rho_s$), where λ_{ab} is the in-plane penetration depth and ρ_s is the superfluid density. The degree of free energy barrier tilting depends on how large I_m is in comparison with the intrinsic circulating current, I_s, which depends on ρ_s (not known for Sr_2RuO_4). A large j_c should be a good indication of a large ρ_s (true for an s-wave superconductor [1]). Both samples B and E were found to possess a very large J_c (Table I), making trapping of HQV likely. Indeed, secondary peaks in MR oscillations which are not as prominent as those in sample B were observed in sample E, but only in a narrow range of small I_m, which we believe are also due to fluxoid state trapping (see SM [40] for more details).

IV. DISCUSSION

A. Experimental detection of HQV fluxoid states

The idea of detecting the HQV fluxoid state by mapping HQV features in the free energy of the system to MR oscillations is similar to that used in the original magnetometry experiment, in which the c-axis magnetization, which is proportional to the derivative of the free energy with respect to Φ, was measured [14]. The transition from the FQV to the HQV fluxoid state corresponds to a jump in the magnetization [or I_s; see Fig. 4(c), upper panel], which is a sharp feature so long that the tiny magnetization can be detected to begin with. On the other hand, the mapping from a small peak seen in Fig. 4(f) (upper panel) using Eq. (1) does not produce a comparably sharp feature in MR oscillations. In addition, local variations of the free energy in our samples such as those from dislocations as discussed above, structural defects, and/or impurities are superimposed on global features in the Φ-dependent free energy. An in-plane field larger than those used in magnetometry measurements will then be needed to ensure the global features are more prominent than those from local sources for them to be properly mapped into MR oscillations and observed experimentally. On the other hand, the control offered by I_m, which was not available in the original magnetometry experiment, provides us with additional insights into the HQV physics not available previously.

The presence of both in-plane and c-axis magnetic fields makes the total magnetic field at an angle with the in-plane direction, which opens the possibility that the magnetic flux can enter from one end of the cylinder, be enclosed in its interior, and then exit through the cylinder wall (as an Abrikosov FQV) instead of the other end. Such sidewall conventional FQVs will in principle also give rise to the half-height jumps seen in the original magnetometry experiment. However, in this scenario, the FQV must exit from the sidewall exactly halfway of the cylinder to account for data seen in every sample that was studied, which is unlikely. Indeed, the measurements on control samples of a conventional superconductor of $NbSe_2$ did not reveal such half-height jumps seen in Sr_2RuO_4 samples. Numerical modeling showed that the in-plane field used in the magnetometry experiment was below the lower critical field for samples used in that study and a sidewall FQV forced into the sample is never stable [41]. As a result, the sidewall scenario seems to be unlikely to be responsible for the experimental signatures that were attributed to the HQV fluxoid state.

As illustrated in Fig. 4, lowering the HQV free-energy parabolas from geometrical constraints and the in-pane magnetic field will make both the FQV and HQV fluxoid state the ground state at various Φ values. In the LP experiment, the free-energy landscape is mapped into T_c oscillations [4], which are measured typically by tracking the temperature at which a fixed value of sample resistance is obtained in the superconducting transition regime. It was reported in Ref. [45] that MR oscillations observed in two square loops of single-crystal Sr_2RuO_4 of mesoscopic size in the presence of an in-plane field were due to the LP effect. However, we believe that MR oscillations observed in that work are actually due to vortex crossings as well (see more discussion in the SM [40]).

In-plane Abrikosov FQVs and perhaps HQVs as well can also form in our samples when the in-plane field is sufficiently large. These in-plane vortices are expected to stay away from the two singly connected parts of the sample (between the cylinder and a voltage lead) because they are near multiple branching of a mesoscopic sample where the local energy gap tends to be enhanced [42,43]. The crossing of in-plane FQV/HQV vortices through the doubly connected part of the sample will be subject to the same free-energy barrier for the c-axis vortex crossing, which should not lead to any new features in MR oscillations.

B. Stability of HQV

Experimental observations presented above appear to suggests that a large J_c value favors the stability of the HQV fluxoid state. In the absence of $H_{||ab}$, the free-energy difference between a HQV fluxoid state and that of FQV at $\Phi = (m + \frac{1}{2})\Phi_0$ is proportional to $(\rho_{sp}/\rho_s) - (1+\beta)^{-1}$. Only when $\beta < \rho_s/\rho_{sp} - 1$ is the HQV stable. Given that β itself is proportional to ρ_s, whether a large ρ_s in similarly sized samples will help the stability of the HQV depends on how ρ_{sp} and ρ_s are related to one another. Their relationship was analyzed for bulk superfluid ^{3}He [7]. Unfortunately, for a spin-triplet superconductor, how ρ_s and ρ_{sp} are related to one another is not known. Experimentally, it is difficult to perform measurements on ρ_s even in the bulk, let alone for a mesoscopic sample. In any case, if ρ_{sp} and ρ_s are relatively independent, a large ρ_s may indeed be connected to a large J_c, which will in turn favor the formation of spin counterflow HQV fluxoid state.

The above assessment on the role played by J_c in the stability of HQV appears to be supported by MR oscillation results obtained from not only samples featuring a large J_c value (discussed above) but also ones with a small J_c. As discussed in more detail in the SM [40], MR oscillation measurements on a cylinder, sample HL, featuring small J_c, support this

picture. This sample possesses a cylinder radius and a wall thickness similar to other samples but a height larger than them (Table I). Because the free-energy barrier is proportional to the cylinder length, the large height would imply that vortex crossings in this sample are more difficult than other samples. Nevertheless, MR oscillations with a period of Φ_0 were readily observed. However, the dip feature was often found to be missing even under a large $H_{||ab}$ (see SM [40]).

C. Implications of the observation of HQV

The observation of the HQV fluxoid state in single-crystal, mesoscopic Sr_2RuO_4 in the original magnetometry and the present experiment is explained most naturally in the spin-triplet pairing picture. However, a spin-singlet single-crystal structure can also host a HQV fluxoid state (but not a spin counterflow one) if it possesses a two-component OP, which can emerge from accidental degeneracy of two pairing states, which will lead to TRSB as mentioned above. On the other hand, fractional quantum vortices should also form, perhaps more frequently than HQV [13]. Experimentally, no signs of a fractional quantum vortex were detected in the original magnetometry [14] and present MR oscillation measurements, making it unlikely that the observed HQV is due to a two-component OP.

Spontaneous half-quantum flux can also emerge in various GLB structures of either a spin-singlet or a spin-triplet superconductor. Because of the π-phase jump over one of the two Josephson junctions in the GLB SQUID [29], the phase winding accumulated by the phase gradient away from the junctions will be π, leading to the trapping of magnetic flux of $\frac{1}{2}\Phi_0$, which we refer to as GLB HQV. Experimentally, in addition to the $Au_{0.5}In_{0.5}$-Sr_2RuO_4 GLB SQUID discussed above [30], GLB structures of spin-singlet, d-wave superconductor of high-T_c cuprates [46–48], hybrid Nb-granular iron pnictide loops [49], and granular rings of β-Bi_2Pd [50] were found to show the presence of GLB HQV. Importantly, none of these structures is a single-crystal one, making the GLB HQV fundamentally different from the spin counterflow HQV fluxoid state.

The formation of the spin counterflow HQV fluxoid state due to a spin-triplet pairing symmetry in mesoscopic Sr_2RuO_4 under a sufficiently large $H_{||ab}$ suggests that the SSP is along the in-plane direction. However, whether this has implications on the orientation of the d-vector in the bulk or even a mesoscopic sample of Sr_2RuO_4 depends on how the HQV is formed microscopically. In the Vakaryuk-Leggett picture based on an ESP state, in which a uniform SSP is formed, the d-vector must be along the c axis at least in a mesoscopic sample in which the influence of the sample surface is important. In this picture, the SSP will be along the ab plane perpendicular to the d-vector [8], allowing an $H_{||ab}$ to help stabilize HQV. As stated above, the new Knight shift and PNS results seem to suggest that the bulk Sr_2RuO_4 cannot be in the chiral p-wave (Γ_5^-) state with the d-vector along the c axis. However, even if the bulk Sr_2RuO_4 is in one of the helical spin-triplet states (Γ_{1-4}^-) with the d-vector along the ab plane, a substantial c-axis component of the d-vector can still be obtained by rotating the in-plane d-vector in a helical state near the surface, allowed by the loss of the bulk crystalline symmetry near the boundary as well as a dipole-dipole interaction [13]. This will also explain the apparent c-axis oriented d-vector seen in the Josephson effect experiments (including the phase-sensitive experiment) suggesting a d-vector that has a substantial c-axis component. Alternatively, an in-plane SSP can come from the d-soliton which can form even if the d-vector away from the soliton is not along the c axis, as mentioned above. Combining the Josephson effect and HQV measurements, most likely the d-vector is along the c axis near the surface of bulk Sr_2RuO_4 and in mesoscopic samples of this superconductor.

The spin counterflow HQV is expected to possess a single Majorana zero-energy mode (MZEM) [51], useful for fault-tolerant topological quantum computation (TQC) [52]. In the Γ_5^- state featuring TRSB, MZEM can emerge as a core state of Abrikosov HQV. For any one of the helical states (Γ_{1-4}^-), even though the time-reversal symmetry is not broken for the whole system, each spin species of the condensate does break it. Since the HQV forms only in one of the two spin species at least within the ESP picture, MZEM should still exist in the HQV [13]. To implement TQC, braiding operations of MZEMs are necessary. Given that MZEMs are charge neutral, moving MZEMs around one another for braiding operations is difficult to implement. An Abrikosov HQV may be moved around in the sample by a current-induced Lorentz force as well as by a scanning SQUID [53] or point-contact probe [54], making MZEMs bound to an Abrikosov HQV potentially advantageous over other MZEMs for implementing TQC.

V. CONCLUSIONS

To conclude, we performed MR oscillation measurements on doubly connected, single-crystal cylinders of Sr_2RuO_4 of a mesoscopic size in the presence of a large in-plane magnetic field. These measurements revealed distinct features, including a dip and secondary peak in MR oscillations, which support the formation of spin counterflow HQV fluxoid states in these samples as well as an odd-parity, spin-triplet pairing symmetry in Sr_2RuO_4. The establishment of spin counterflow HQV revealed an additional analog between superconducting Sr_2RuO_4 and superfluid ^{3}He given the recent observation of HQV in the latter, in which geometrical constraints also play an important role in stabilizing HQV [55]. Finally, this work provides insights into the stability of HQV and the d-soliton picture of HQV. Important issues to be investigated in the future include the quantitative determination of SSP and ρ_{sp}, direct imaging of HQV, and the potential use of HQV for fault-tolerant TQC.

ACKNOWLEDGMENTS

We would like to thank A. J. Leggett, V. Vakaryuk, S.-K. Chung, K. Roberts, Y. Maeno, J. Kirtley, C. Kallin, J. A. Sauls, J. K. Jain, Z. Wang, and W. Huang for useful discussions. We would also like to express our gratitude to the referees for their critical review of our manuscript and constructive suggestions. The work at Penn State was supported by DOE under Grant No. DE-FG02-04ER46159. Z.Q.M. acknowledges the support by NSF under Grant No. DMR 1917579.

[1] M. Tinkham, *Introduction to Superconductivity*, 2nd ed. (McGraw-Hill, New York, 1996).

[2] B. S. Deaver and W. M. Fairbank, Experimental Evidence for Quantized Flux in Superconducting Cylinders, Phys. Rev. Lett. **7**, 43 (1961).

[3] R. Doll and M. Näbauer, Experimental Proof of Magnetic Flux Quantization in a Superconducting Ring, Phys. Rev. Lett. **7**, 51 (1961).

[4] W. A. Little and R. D. Parks, Observation of Quantum Periodicity in the Transition Temperature of a Superconducting Cylinder, Phys. Rev. Lett. **9**, 9 (1962).

[5] G. E. Volovik and V. P. Mineev, Line and point singularities in superfluid He^3, JETP Lett. **24**, 561 (1976).

[6] M. C. Cross and W. F. Brinkman, Textural singularities in the superfluid A phase of ^{3}He, J. Low Temp. Phys. **27**, 683 (1977).

[7] A. J. Leggett, A theoretical description of the new phases of liquid ^{3}He, Rev. Mod. Phys. **47**, 331 (1975).

[8] V. Vakaryuk and A. J. Leggett, Spin Polarization of Half-Quantum Vortex in Systems with Equal Spin Pairing, Phys. Rev. Lett. **103**, 057003 (2009).

[9] H.-Y. Kee, Y. B. Kim, and K. Maki, Half-quantum vortex and $\hat{d}$-soliton in Sr_2RuO_4, Phys. Rev. B **62**, R9275 (2000).

[10] S. B. Chung, H. Bluhm, and E.-A. Kim, Stability of Half-Quantum Vortices in $p_x + ip_y$ Superconductors, Phys. Rev. Lett. **99**, 197002 (2007).

[11] H.-Y. Kee and K. Maki, Half quantum vortex in superfluid ^{3}He-A phase in parallel-plate geometry, Europhys. Lett. **80**, 46003 (2007).

[12] H.-Y. Kee and M. Sigrist, Releasing half-quantum vortices via the coupling of spin polarization, charge- and spin-current, arXiv:1307.5859.

[13] A. J. Leggett and Y. Liu, Symmetry properties of superconducting order parameter in Sr_2RuO_4, J. Supercond. Novel Magn. **34**, 1647 (2021).

[14] J. Jang, D. G. Ferguson, V. Vakaryuk, R. Budakian, S. B. Chung, P. M. Goldbart, and Y. Maeno, Observation of half-height magnetization steps in Sr_2RuO_4, Science **331**, 186 (2011).

[15] T. M. Rice and M. Sigrist, Sr_2RuO_4: An electronic analogue of ^{3}He? J. Phys.: Condens. Matter **7**, L643 (1995).

[16] G. Baskaran, Why is Sr_2RuO_4 not a high-T_c superconductor? Electron correlation, Hund's coupling and p-wave instability, Physica B (Amsterdam) **223-224**, 490 (1996).

[17] Y. Maeno, H. Hashimoto, K. Yoshida, S. Nishizaki, T. Fujita, J. G. Bednorz, and F. Lichtenberg, Superconductivity in a layered perovskite without copper, Nature (London) **372**, 532 (1994).

[18] A. P. Mackenzie and Y. Maeno, The superconductivity of Sr_2RuO_4 and the physics of spin-triplet pairing, Rev. Mod. Phys. **75**, 657 (2003).

[19] I. Eremin, D. Manske, S. G. Ovchinnikov, and J. F. Annett, Unconventional superconductivity and magnetism in Sr_2RuO_4 and related materials, Ann. Phys. **13**(3), 149 (2004).

[20] Y. Maeno, S. Kittaka, T. Nomura, S. Yonezawa, and K. Ishida, Evaluation of spin-triplet superconductivity in Sr_2RuO_4, J. Phys. Soc. Jpn. **81**, 011009 (2012).

[21] C. Kallin, Chiral p-wave order in Sr_2RuO_4, Rep. Prog. Phys. **75**, 042501 (2012).

[22] Y. Liu and Z.-Q. Mao, Unconventional superconductivity in Sr_2RuO_4, Physica C (Amsterdam) **514**, 339 (2015).

[23] K. Ishida, H. Mukuda, Y. Kitaoka, K. Asayama, Z. Q. Mao, Y. Mori, and Y. Maeno, Spin-triplet superconductivity in Sr_2RuO_4 identified by ^{17}O Knight shift, Nature (London) **396**, 658 (1998).

[24] J. A. Duffy, S. M. Hayden, Y. Maeno, Z. Mao, J. Kulda, and G. J. McIntyre, Polarized-Neutron Scattering Study of the Cooper-Pair Moment in Sr_2RuO_4, Phys. Rev. Lett. **85**, 5412 (2000).

[25] A. Pustogow, Y. Luo, A. Chronister, Y.-S. Su, D. A. Sokolov, F. Jerzembeck, A. P. Mackenzie, C. W. Hicks, N. Kikugawa, S. Raghu, E. D. Bauer, and S. E. Brown, Constraints on the superconducting order parameter in Sr_2RuO_4 from oxygen-17 nuclear magnetic resonance, Nature (London) **574**, 72 (2019).

[26] K. Ishida, M. Manago, K. Kinjo, and Y. Maeno, Reduction of the ^{17}O Knight shift in the superconducting state and the heat-up effect by NMR pulses on Sr_2RuO_4, J. Phys. Soc. Jpn. **89**, 034712 (2020).

[27] A. N. Petsch, M. Zhu, M. Enderle, Z. Q. Mao, Y. Maeno, I. I. Mazin, and S. M. Hayden, Reduction of the Spin Susceptibility in the Superconducting State of Sr_2RuO_4 Observed by Polarized Neutron Scattering, Phys. Rev. Lett. **125**, 217004 (2020).

[28] A. Chronister, N. Pustogow, A. Kikugawa, D. A. Sokolov, F. Jerzembeck, C. W. Hicks, A. P. Mackenzie, E. D. Bauer, and S. E. Brown, Evidence for even parity unconventional superconductivity in Sr_2RuO_4, Proc. Natl. Acad. Sci. USA **118**, e2025313118 (2021).

[29] V. B. Geshkenbein, A. I. Larkin, and A. Barone, Vortices with half magnetic flux quanta in "heavy-fermion" superconductors, Phys. Rev. B **36**, 235 (1987).

[30] K. D. Nelson, Z.-Q. Mao, Y. Maeno, and Y. Liu, Odd-parity superconductivity in Sr_2RuO_4, Science **306**, 1151 (2004).

[31] V. Vakaryuk and V. Vinokur, Effect of Half-Quantum Vortices on Magnetoresistance of Perforated Superconducting Films, Phys. Rev. Lett. **107**, 037003 (2011).

[32] X. Cai, Y. A. Ying, N. E. Staley, Y. Xin, D. Fobes, T. J. Liu, Z.-Q. Mao, and Y. Liu, Unconventional quantum oscillations in mesoscopic rings of spin-triplet superconductor Sr_2RuO_4, Phys. Rev. B **87**, 081104(R) (2013).

[33] R. P. Groff and R. D. Parks, Fluxoid quantization and field-induced depairing in a hollow superconducting microcylinder, Phys. Rev. **176**, 567 (1968).

[34] Y. A. Ying, N. E. Staley, Y. Xin, K. Sun, X. Cai, D. Fobes, T. J. Liu, Z. Q. Mao, and Y. Liu, Enhanced spin-triplet superconductivity near dislocations in Sr_2RuO_4, Nat. Commun. **4**, 2596 (2013).

[35] I. Sochnikov, A. Shaulov, Y. Yeshurun, G. Logvenov, and I. Božović, Large oscillations of the magnetoresistance in nanopatterned high-temperature superconducting films, Nat. Nanotechnol. **5**, 516 (2010).

[36] G. R. Berdiyorov, M. V. Milošević, M. L. Latimer, Z. L. Xiao, W. K. Kwok, and F. M. Peeters, Large Magnetoresistance Oscillations in Mesoscopic Superconductors due to Current-Excited Moving Vortices, Phys. Rev. Lett. **109**, 057004 (2012).

[37] S. A. Mills, C. Shen, Z. Xu, and Y. Liu, Vortex crossing and trapping in doubly connected mesoscopic loops of a single-crystal type-II superconductor, Phys. Rev. B **92**, 144502 (2015).

[38] V. Ambegaokar and B. I. Halperin, Voltage Due to Thermal Noise in the dc Josephson Effect, Phys. Rev. Lett. **22**, 1364 (1969).

[39] V. G. Kogan, J. R. Clem, and R. G. Mints, Properties of mesoscopic superconducting thin-film rings: London approach, Phys. Rev. B **69**, 064516 (2004).

[40] See Supplemental Material at http://link.aps.org/supplemental/10.1103/PhysRevB.105.224510.

[41] K. Roberts, R. Budakian, and M. Stone, Numerical study of the stability regions for half-quantum vortices in superconducting Sr_2RuO_4, Phys. Rev. B **88**, 094503 (2013).

[42] H. J. Fink and V. Grünfeld, Critical current of thin superconducting wire with side branches, Phys. Rev. B **31**, 600 (1985).

[43] H. Wang, M. M. Rosario, H. L. Russell, and Y. Liu, Observation of double resistance anomalies and excessive resistance in mesoscopic superconducting $Au_{0.7}In_{0.3}$ rings with phase separation, Phys. Rev. B **75**, 064509 (2007).

[44] Y. Maeno, T. Ando, Y. Mori, E. Ohmichi, S. Ikeda, S. NishiZaki, and S. Nakatsuji, Enhancement of Superconductivity of Sr_2RuO_4 to 3 K by Embedded Metallic Microdomains, Phys. Rev. Lett. **81**, 3765 (1998).

[45] Y. Yasui, K. Lahabi, M. S. Anwar, Y. Nakamura, S. Yonezawa, T. Terashima, J. Aarts, and Y. Maeno, Little-Parks oscillations with half-quantum fluxoid features in Sr_2RuO_4 microrings, Phys. Rev. B **96**, 180507(R) (2017).

[46] D. J. Van Harlingen, Phase-sensitive tests of the symmetry of the pairing state in the high-temperature superconductors—evidence for $d_{x^2-y^2}$ symmetry, Rev. Mod. Phys. **67**, 515 (1995).

[47] C. C. Tsuei and J. R. Kirtley, Pairing symmetry in cuprate superconductors, Rev. Mod. Phys. **72**, 969 (2000).

[48] C. W. Schneider, G. Hammerl, G. Logvenov, T. Kopp, J. R. Kirtley, P. J. Hirschfeld, and J. Mannhart, Half-*h*/2e critical current—oscillations of SQUIDs, Europhys. Lett. **68**, 86 (2004).

[49] C.-T. Chen, C. C. Tsuei, M. B. Ketchen, Z.-A. Ren, and Z. X. Zhao, Integer and half-integer flux-quantum transitions in a niobiumiron pnictide loop, Nat. Phys. **6**, 260 (2010).

[50] Y. Li, X. Xu, M.-H. Lee, M.-W. Chu, and C. L. Chien, Observation of half-quantum flux in the unconventional superconductor β-Bi_2Pd, Science **366**, 238 (2019).

[51] S. Das Sarma, C. Nayak, and S. Tewari, Proposal to stabilize and detect half-quantum vortices in strontium ruthenate thin films: Non-Abelian braiding statistics of vortices in a $p_x + ip_y$ superconductor, Phys. Rev. B **73**, 220502(R) (2006).

[52] C. Nayak, S. H. Simon, A. Stern, M. Freedman, and S. Das Sarma, Non-Abelian anyons and topological quantum computation, Rev. Mod. Phys. **80**, 1083 (2008).

[53] E. W. J. Straver, J. E. Hoffman, O. M. Auslaender, D. Rugar, and K. A. Moler, Controlled manipulation of individual vortices in a superconductor, Appl. Phys. Lett. **93**, 172514 (2008).

[54] A. Kremen, S. Wissberg, N. Haham, E. Persky, Y. Frenkel, and B. Kalisky, Mechanical control of individual superconducting vortices, Nano Lett. **16**, 1626 (2016).

[55] S. Autti, V. V. Dmitriev, J. T. Mäkinen, A. A. Soldatov, G. E. Volovik, A. N. Yudin, V. V. Zavjalov, and V. B. Eltsov, Observation of Half-Quantum Vortices in Topological Superfluid ^{3}He, Phys. Rev. Lett. **117**, 255301 (2016).